Seismoacoustic coupling induced by the breakup of the 15 February 2013 Chelyabinsk meteor

Benoit Tauzin, Eric Debayle, Cathy Quantin, Nicolas Coltice

Seismoacoustic coupling induced by the breakup of the 15 February 2013 Chelyabinsk meteor

Benoit Tauzin,[1] Eric Debayle,[1] Cathy Quantin,[1] and Nicolas Coltice[1]

Received 15 April 2013; revised 18 June 2013; accepted 18 June 2013.

[1] On 15 February 2013 around 03:20:00 UTC, the largest meteor reported since the 1908 Tunguska event was observed as a fireball traveling through the Earth's atmosphere, exploding in an air burst near the city of Chelyabinsk, Russia. The rarity of such an event provides a unique window on the physics of meteoroid collision. We report the fine seismic detection of Rayleigh waves produced by the coupling of ground motion with the incident shock wave at distances up to 4000 km from the event. Combining information from seismic beam-forming analysis, reconstructed trajectory from casual video records, and remote sensing, we identify the Rayleigh waves as being initiated by the shock wave produced by the main blast that occasioned damages and injuries in Chelyabinsk. From the Rayleigh wave observations, we report a magnitude $M_s \sim 3.7$ seismic source. **Citation:** Tauzin, B., E. Debayle, C. Quantin, and N. Coltice (2013), Seismoacoustic coupling induced by the breakup of the 15 February 2013 Chelyabinsk meteor, *Geophys. Res. Lett.*, *40*, doi:10.1002/grl.50683.

1. Introduction

[2] The Chelyabinsk meteor is the largest recorded object that entered the Earth's atmosphere since the Tunguska event in 1908 [*Ben-Menahem*, 1975]. It generated on its way multiple blast events due to meteor fragmentation. The largest was reported by the NASA Near-Earth Object Program (http://neo.jpl.nasa.gov) at about 23 km altitude and is thought to have caused injuries and damages within the city of Chelyabinsk. Multiple fragments of the meteor have also been reported to hit the ground, the largest in the region of the lake Chebarkul, 70 km west-south west of Chelyabinsk. These fragments, millimeters to centimeters in size, are however likely too small to generate seismic waves that can be detected a few hundred kilometers away [*Edwards et al.*, 2007].

[3] Seismic waves are more commonly generated by the sonic shock wave associated with the meteor [*Anglin and Haddon*, 1987]. When a meteor enters the Earth's atmosphere at hypersonic velocities, it produces a ballistic shock wave within a narrow Mach cone. The induced pressure wave propagates with a wavefront that can be approximated as cylindrical [e.g., *ReVelle*, 1976]. Additional shock waves with quasi-spherical wavefronts can also be produced by the meteor fragmentation. These shock waves, though experiencing frequency-dependent attenuation as they propagate in the atmosphere, could be detected in the case of Cheylabinsk as infrasound waves recorded at sensors of the Comprehensive Nuclear Test Ban Treaty all over the world [*Le Pichon et al.*, 2013]. These infrasounds impinge the Earth's surface with sufficient energy to induce a measurable seismic signal [*Edwards et al.*, 2007].

[4] In this study, we show that coupling between the meteor's shock wave and ground motion produces Rayleigh waves that can be detected at distances up to 4000 km from Chelyabinsk. These Rayleigh waves can be used to infer the deep internal structure of the Earth. Such Rayleigh waves, precursory to the ground motion associated with the meteor's shock wave, have so far been rarely observed.

2. Seismic Data Analysis

[5] We analyze 2016 three-component broadband seismograms recorded at seismic stations of the Global Seismographic Network and the International Federation of Digital Seismographic Networks (Figure 1). Among them, we use 73 vertical components recorded at distances up to 4000 km from the Chelyabinsk city (red stations in the map of Figure 1). In Figure 1, these seismograms are sorted by increasing distance and band-pass filtered in the period range 20–60 s. The extraction of the seismic signal associated with the Chelyabinsk meteor is significantly blurred by the coincidental interference with seismic waves of a magnitude 5.8 earthquake that occurred 20 min earlier in the Tonga archipelago (Figure 1). Figure S1 in the supporting information provides a zoomed image of the distance ranging from 0 to 2000 km in Figure 1.

[6] The first arrivals in the seismograms are *P* phases radiated by the Tonga earthquake. Travel times computed for the IASP91 reference velocity model [*Kennett and Engdahl*, 1991] as well as synthetic seismograms computed in a 3-D Earth [*Tromp et al.*, 2010] (Figure S2) indicate the presence of core phases (PKP and PKIKP) as well as *P* phases reflected under the surface of the Earth (PP). The strongest signal is a dispersed wave train which is framed by the gray curves in Figure 1. This wave train can hardly be explained by the earthquake. First, it is not modeled by the simulation in a realistic Earth's model (Figure S2). Second, its arrival time t does not increase linearly with the distance from the Tonga epicenter (Figure S3). Instead, it increases linearly with the distance d from Chelyabinsk (i.e., $t = d/v$ with an apparent constant velocity v) suggesting that it is emitted in this region. It propagates in

Additional supporting information may be found in the online version of this article.

[1]Laboratoire de Géologie de Lyon: Terre, Planète, Environnement, CNRS UMR 5276, Université Lyon 1, Université de Lyon, Ecole Normale Supérieure de Lyon, Villeurbanne, France.

Corresponding author: B. Tauzin, Laboratoire de Géologie de Lyon: Terre, Planète, Environnement, CNRS UMR 5276, Université Lyon 1, Université de Lyon, 2 rue Raphael Dubois, 69622 Villeurbanne Cedex, France. (benoit.tauzin@univ-lyon1.fr)

0094-8276/13/10.1002/grl.50683

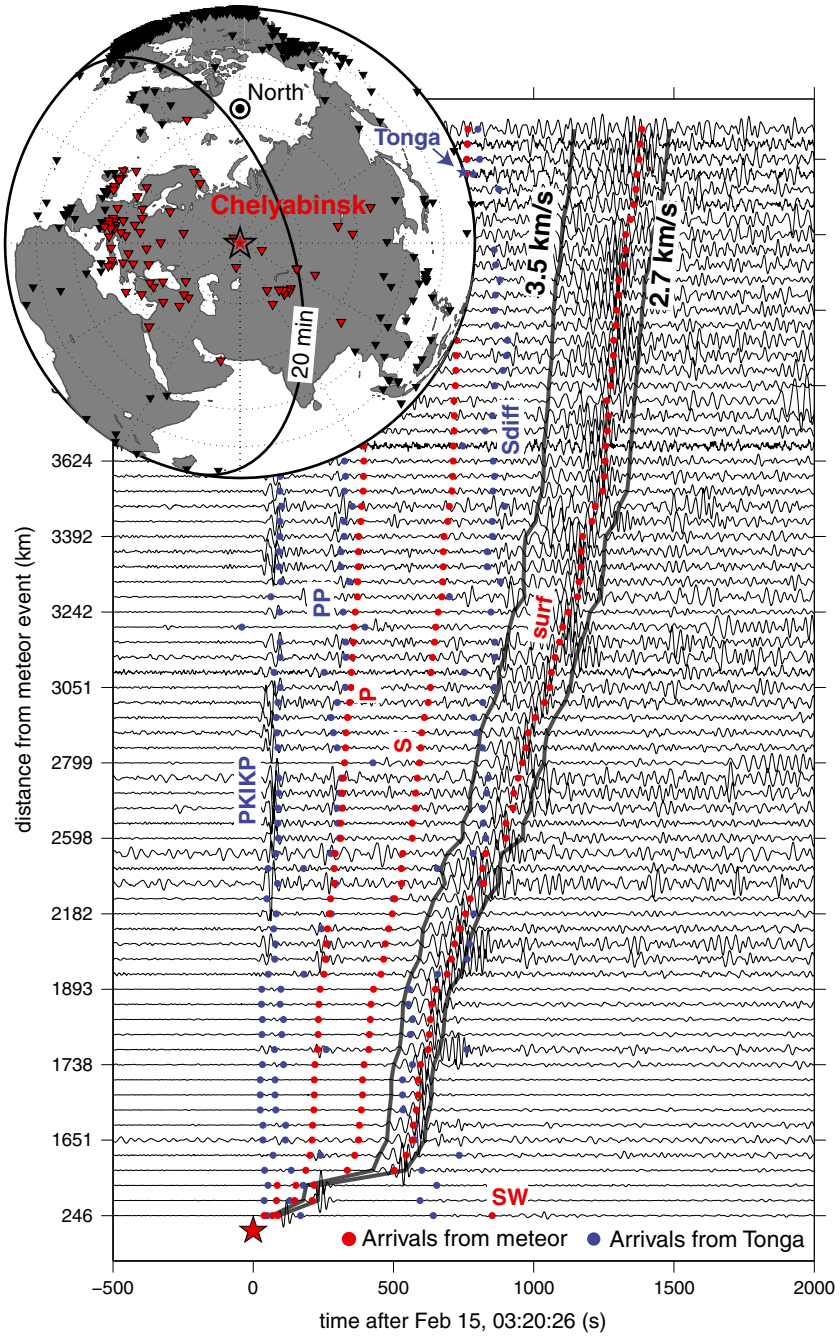

Figure 1. Vertical component seismograms for stations located within ±4000 km from the city of Chelyabinsk. The seismograms are band-pass filtered between 20 and 60 s. The origin time is the time proposed for the main meteor blast (i.e. t_0 = 03:20:36 UTC). Along the *Y* axis, the data are sorted by increasing distance from the reported burst point in this study (54.82°N, 61.24°E). Note that distance is not increasing linearly along this axis. Body waves (PKIKP, PP, and Sdiff) from the Tonga earthquake are indicated with blue dots. The gray curves delineate inferred Rayleigh waves associated with the Chelyabinsk meteor. They correspond to curves $t = t_0 + d/v$ with v = 3.5 and 2.7 km/s, respectively. Predicted travel times for *P*, *S*, surface waves, and shock waves (SW) induced by the meteor event are indicated with red dots. The map at the top left shows the location of the city of Chelyabinsk (red star) with all broadband seismological stations within 4000 km (red triangles) and away (black triangles). The North Pole is indicated with a double black circle. A 20 min travel time isocontour for *P* waves emitted by the Tonga earthquake is indicated as a black small circle on the sphere.

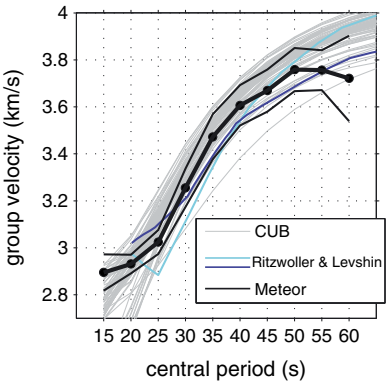

Figure 2. Dispersion curve (black lines) obtained from narrowband-pass filtering the data recorded within 4000 km from Chelyabinsk at different central periods and applying our "delay and sum" approach. The central thick black curve is the average dispersion curve $v_a(T)$. The upper and lower black curves delimit the 95% confidence level. Group velocity curves computed for the fundamental mode of Rayleigh waves propagating between each source receiver pairs in the CUB model [*Shapiro and Ritzwoller*, 2002] and observed for Eurasian shields/platforms by *Ritzwoller and Levshin* [1998] are indicated as gray and blue lines, respectively.

the ground with an apparent velocity between 2.7 and 3.5 km/s (Figure 1, gray curves). The wave train is unambiguously identified as Rayleigh waves by the dispersion of the signal with frequency and the recorded elliptical retrograde ground motions occurring essentially in the vertical plane (Figure S4 in the supporting information). Waves from Tonga, although interfering, are weaker by 1 or 2 orders of magnitude (Figure S5). Our observations of absolute travel times, particle motion, and dispersion thus suggest that we isolated meteor-induced Rayleigh waves among waveforms associated with the Tonga earthquake.

[7] We have extracted the average group velocity dispersion for these Rayleigh waves (Figure 2). We band-pass filter the seismograms of Figure 1 from 15 to 60 s by step of 5 s period. We take the envelope of the signals and apply a "delay and sum" approach, i.e., stack these envelopes along linear curves of equation $t = d/v + t_0$, with d the distance from Chelyabinsk. We test values of v within 2.5 km/s and 5 km/s. The result is a time-velocity diagram (Figure S6) whose maximum indicates the origin time $t_0(T)$ and the group velocity $v(T)$ for Rayleigh waves at period T. We use a bootstrap resampling approach [*Efron and Tibshirani*, 1991] to estimate the average dispersion and its associated error. The obtained dispersion relation is classical with longer wavelengths or periods arriving before shorter wavelengths (Figure 2). Indeed, the S wave velocity generally increases with depth in the uppermost 100 km of continents and Rayleigh waves measure a weighted average of the S wave structure over a depth interval that increases with period. Comparison with dispersion curves for the same region [*Ritzwoller and Levshin*, 1998; *Shapiro and Ritzwoller*, 2002] confirms that the measured dispersion is typical of a fundamental Rayleigh mode propagating within a Precambrian lithosphere (Figure 2). This is a nice example of how a meteor-induced Rayleigh wave can be used to infer the internal structure of a planetary body with an atmosphere.

[8] We relocate the source emission of meteor-induced Rayleigh waves using the dispersion relation relating group velocity to frequency and a similar approach developed by *Lay* [1987] to illuminate near-source structures from teleseismic P waves generated by underground explosions. We use a spatial grid around Chelyabinsk of 1501 × 1501 km with ∼1 km wide cells. Assuming an origin time for the meteor event (with uncertainties $t_0(T)$ on this time considered here), the amplitude at each predicted travel time from a given grid point is taken on the envelope of the corresponding vertical component seismogram. These amplitudes are then backprojected onto the corresponding grid points. By

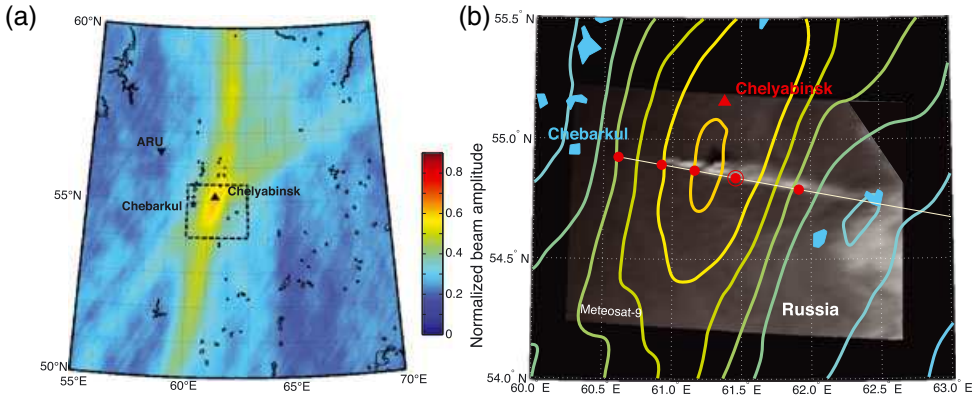

Figure 3. (a) Result of the beam stack migration of 15 s period envelopes of vertical component seismograms recorded at stations within 4000 km from Chelyabinsk. The city of Chelyabinsk, the lake Chebarkul, and the closest seismic station ARU are indicated with a triangle, a star, and an inverted triangle, respectively. The dashed square delineates the region depicted in Figure 3b. (b) Superimposition of contours obtained from the seismic beam-forming over the Meteosat-9 satellite image. The color code for beam contours is the same as in Figure 3a. The trajectory estimated from casual video records (IAU telegram) is indicated in yellow with the four successive flares as red dots. The main blast is indicated with a double dot. Before projection, the satellite image has been rectified using altitudes giving a vapor trail trajectory collinear with the probable impact site of the Chebarkul Lake. The trajectories inferred from satellite and video records are close to each other. Our maximum of beam amplitude is located at (54.82°N, 61.24°E).

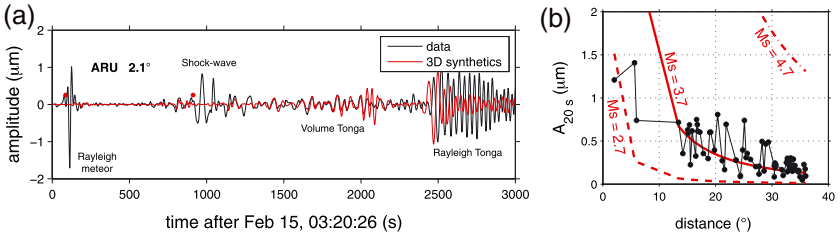

Figure 4. (a) Observation of the shock wave associated with the Chelyabinsk event. The comparison of the 3-D synthetic and the observed seismogram at ARU station reveals in addition to the Rayleigh waves a W-shaped wave train at an arrival time (red dot) predicted for the meteor-induced shock wave. This wave train is produced by seismoacoustic coupling at ARU station, in contrast to the Rayleigh wave induced by the meteor which has been generated from seismoacoustic coupling in the close vicinity of the meteor ground-projected trajectory. (b) Measurements (black dots) of the amplitude of ground motion in μm as a function of the distance from the blast location. These measurements are the maximum amplitude of Rayleigh waves recorded on the vertical components of stations within 4000 km from Chelyabinsk. The seismograms have been deconvolved from the instrument response and filtered with a Gaussian filter centered at 20 s period. The red curves are the theoretical curves for seismic events of magnitudes M_s 2.7, 3.7, and 4.7 estimated with the Prague formula. There is an ambiguity at close stations where the estimated magnitude appears closer to 2.7. We checked that the interference of seismic waves from Tonga could not significantly amplify the recovered ground motion at large distances. We estimated amplitude corrections from the amplitudes measured on the 3-D synthetic seismograms (Figure S5 in the supporting information). These corrections were found rarely exceeding 20% of the measured Rayleigh amplitudes and have no impact on the recovered magnitude for the meteoritic event. The explanation for anomalous values of magnitude at the closest stations must thus come from the validity of the Prague relation limited to events at distances greater than 15°.

averaging the amplitudes taken from the envelopes of all vertical component seismograms, we produce for every period of Rayleigh wave a map of normalized beam amplitude (Figure S7). The maximum in beam amplitude indicates the best estimate for the location of emission of seismic waves. Our higher-resolution map obtained from the backprojection of 15 s period Rayleigh waves is shown in Figure 3a. The maximum is located south of the city of Chelyabinsk. The resolution is <100 km in the ESE-WNW, but poorer in the NNE-SSW direction, as most stations for which Rayleigh waves could be observed (red stations in the map of Figure 1) are located east or west to Chelyabinsk. This is confirmed by a simple test of beam-forming synthetic seismic signals (Figure S8).

3. Trajectory From Casual Video Records and Remote Sensing

[9] In a telegram from the International Astronomical Union (IAU), the Astronomical Institute of the Academy of Science, Ondrejov, Czech Republic, reconstructed the meteor trajectory in the atmosphere from seven casual video records. Assuming a trajectory collinear with the probable impact site of Chebarkul Lake, they reported the locations of four successive blasts in an ESE-WNW direction south of 55°N latitude (Figure 3b). We corroborate this trajectory using images from Meteosat-7 and Meteosat-9 that have captured the vapor trail left by the bolide in the atmosphere. These two geostationary meteorological satellites are respectively centered at the longitudes of 57.5°E and 0°E. We rectified and projected the acquired satellite images from the elevation of the trail (Figure S9). We used SEVIRI image in Level 1.0 from Meteosat-7 to compute possible vapor trail trajectories. Meteosat-7 images were preferred as closer to the longitude of the meteor event. We tested elevations between 40 km and 55 km for the eastern extremity of the trail and between 10 and 25 km for the western end. The best match, collinear with the impact site of the Chebarkul Lake, is a vapor trail extending from 45 km altitude to the east to 18 km to the west. The meteor trajectory intersects our broad maximum of seismic beam forming which contains the four blasts (Figure 3b). Seismic beam-forming, casual video records, and remote sensing concur with the main blast (Figure 3b, double red dot) that occasioned damages and injuries in Chelyabinsk being the seismic initiator for the seismic Rayleigh waves.

4. Discussion and Conclusion

[10] The theory of coupling between infrasound waves and elastic ground motion indicates that *P* and *S* body waves may be initiated as well as Rayleigh waves [see, for example, *Ewing et al.*, 1957, pp. 183 and 220–238]. These waves are generated when and where the sweep velocity of the infrasonic trace at the Earth's surface precisely matches the propagation velocities of the seismic waves. The strong contrast between infrasonic waves that propagate in the air with velocities close to the sound ($c \sim 0.3$ km/s) and seismic waves (Rayleigh, *P*, and *S*) that propagate at least 10 times faster requires a very steep shock front incidence. This requires a seismic source in the close vicinity of the meteor ground-projected trajectory. We observe, however, surface waves at distances up to 4000 km from Chelyabinsk. At these distances, our observed Rayleigh waves must thus arrive as precursors of the shock waves. We looked in the records for the shock wave as well as the *P* and *S* seismic waves. The lack of seismic stations in the close vicinity of the meteor trajectory and the interference with the Tonga earthquake render their identification difficult, even using methods from array seismology [e.g., *Rost and Thomas*, 2002]. However, by comparing the observed waveforms with synthetic seismograms computed in a 3-D Earth [*Tromp et al.*, 2010], we identified the shock wave (Figure 4a) and

possibly the *P* and *S* body waves (Figure S10) at the closest stations from Chelyabinsk.

[11] Few observations of precursory seismic waves to meteor-induced shock waves have been reported up to now. The closest to the Chelyabinsk event is probably the observation of Rayleigh waves of the 1908 Tugunska event that were recorded as far as 5293 km away from its source region [*Ben-Menahem*, 1975]. *Anglin and Haddon* [1987] reported precursory Rayleigh waves associated with a meteoroid above Yellowknife, Canada. *Kanamori et al.* [1991] and *Sorrells et al.* [2002] also reported precursory waves to shock fronts but associated with the re-entry in the atmosphere of the *Columbia* space shuttle.

[12] The shock waves can have two main origins: ballistic within a narrow Mach cone or ablational due to meteor fragmentation. In these prior studies, *Ben-Menahem* [1975] invokes a combination of both, *Anglin and Haddon* [1987] used two orthogonal lines of stations in the vicinity of the meteor track to identify a ballistic shock wave. In the case of the space shuttle studies, it is clear that the shock wave has also a ballistic origin. For the Chelyabinsk meteor, we do not have a dense network of stations near the meteor track. However, there is no clear evidence for a cylindrical symmetry radiation pattern along the projected path of the bolide. As can be seen in Figure 3, the source is not elongated in the ESE-WSW direction of the meteor track although our resolution is good in this direction. Figure 3 would thus be in better agreement with a spherical source due to fragmentation [*Edwards et al.*, 2007].

[13] We estimate an equivalent surface wave magnitude M_s for the Chelyabinsk event (Figure 4b). Using the Praha relation [*Karnik et al.*, 1962] $M_s = \log(A/T) + 1.66 \cdot \log(\Delta) + 3.30$, where A is the amplitude of Rayleigh wave displacement on the vertical component in μm and Δ is the epicentral distance, we find a magnitude $M_s = 3.7 \pm 0.3$. This magnitude, comparable to that ($M_s \sim 5$) of the Tugunska event [*Ben-Menahem*, 1975], would correspond to a release of energy of $\sim 2 \cdot 10^{10}$ J from an equivalent $\sim$5 T TNT. The NASA Near-Earth Object Program reported an approximate initial diameter for the asteroid of 18 m and a rough estimation of the observed total radiated energy by the fireball of about 90 kT. A rough estimate of the ratio between the seismic energy and the energy released within the atmosphere is $\sim 5 \times 10^{-5}$. Such limited efficiency is consistent with results from observations of coupling between aerial acoustic sources and ground motion [e.g., *Brown et al.*, 2002] and similar to what is reported for the Tugunska event [*Toon et al.*, 1997].

[14] Present results that use precursory Rayleigh waves induced by the atmospheric breakup of an asteroid to estimate an equivalent seismic source energy give interesting perspectives for planetary seismological missions. For instance, the NASA mission InSight (Interior Exploration using Seismic Investigations, Geodesy, and Heat Transport) plans to land a seismometer on the surface of Mars to investigate among others, the rate of meteorite impacts. Even if the present atmosphere of Mars is about 150 times thinner than the Earth's, atmospheric breakup of interplanetary meteoroids on Mars is predicted and even observed. *Popova et al.* [2003] predicted atmospheric breakups for bolides smaller than 20 cm in diameter. The recent inventory of fresh Martian impact craters detected between two spacecraft surveys highlights even more atmospheric breakup [*Daubar et al.*, 2013; *Malin et al.*, 2006]. Clusters of impact craters that result from atmospheric breakup are widely observed until 35 m of equivalent crater diameters. Present results thus offer perspectives for impact rate survey on Mars by a seismological space mission.

[15] **Acknowledgments.** This work was supported by a Chaire d'Excellence Fellowship from CNRS. The research has received funding from European Research Council under the European Union'S Seventh Framework Program (PF7/2007-2013)/ERC grant agreement n280168. We thank two anonymous reviewers for their constructive comments. We thank Yanick Ricard for his review and Bertrand Trey for a discussion on present-day impact flux on planetary bodies. We thank the Princeton group for providing 3-D synthetic seismograms calculated based upon the spectral element method. The seismograms have been obtained from the Global ShakeMovie portal (http://global.shakemovie.princeton.edu/). We thank the IRIS and Geoscope Data centers for providing seismological data.

[16] The Editor thanks two anonymous reviewers for their assistance in evaluating this paper.

References

Anglin, F., and R. Haddon (1987), Meteoroid sonic shock-wave-generated seismic signals observed at a seismic array, *Nature*, *328*, 607–609.

Ben-Menahem, A. (1975), Source parameters of the Siberian explosion of June 30, 1908, from analysis and synthesis of seismic signal at four stations, *Phys. Earth Planet. Inter.*, *11*, 1–35.

Brown, P., D. ReVelle, E. Tagliaferri, and A. Hildebrand (2002), An entry model for the Tagish lake fireball using seismic, satellite and infrasound records, *Meteor. Planet. Sci.*, *37*, 661–675.

Daubar, I., A. McEwen, S. Byrne, and C. Dundas (2013), The current Martian cratering rate, *Icarus*, *225*, 506–516.

Edwards, W., D. Eaon, and P. Brown (2007), Seismic observations of meteors: Coupling theory and observations, *Rev. Geoph.*, *46*, 1–21.

Efron, B., and R. Tibshirani (1991), Statistical data analysis in the computer age, *Science*, *253*, 390–395.

Ewing, W., W. Jardetzky, and F. Press (1957), *Elastic Waves in Layered Media*, McGraw-Hill, New York.

Kanamori, H., J. Mori, D. Anderson, and T. Heaton (1991), Seismic excitation by the space shuttle *Columbia*, *Nature*, *349*, 781–782.

Karnik, V., N. Kondorskaya, J. Riznitchenko, E. Savarensky, S. Soloviev, N. Shebalin, J. Vanek, and A. Zatopek (1962), Standardization of the earthquake magnitude scale, *Studia Geophysica et Geodaetica*, *6*, 41–48.

Kennett, B., and E. Engdahl (1991), Travel times for global earthquake location and phase identification, *Geophys. J. Int.*, *105*, 429–465.

Lay, T. (1987), Analysis of near-source contributions to early *P*-wave coda for underground explosions. III. Inversion for isotropic scatterers, *Bull. Seismol. Soc. Am.*, *77*, 1767–1783.

Le Pichon, A., L. Ceranna, C. Pilger, P. Mialle, D. Brown, and P. Herry (2013), 2013 Russian Fireball largest ever detected by CTBTO infrasound sensors, *Geophys. Res. Lett.*, doi:10.1002/grl.50619.

Malin, M., K. Edgett, L. Posiolova, S. McColley, and E. Noe Dobrea (2006), Present impact cratering rate and the contemporary gully activity on Mars: Results of the Mars Global Surveyor extended mission, *Science*, *314*, 1573–1557.

Popova, O., I. Nemtchinov, and W. Hartmann (2003), Bolides in the present and past martian atmosphere and effects on cratering processes, *Earth Planet. Sci. Lett.*, *38*, 905–925.

ReVelle, D. (1976), On meteor generated infrasound, *J. Geophys. Res.*, *81*, 1217–1229.

Ritzwoller, M., and A. Levshin (1998), Eurasian surface wave tomography: Group velocities, *J. Geophys. Res.*, *103*, 4839–4878.

Rost, S., and C. Thomas (2002), Array seismology: Methods and applications, *Rev. Geoph.*, *40*, 1–27.

Shapiro, N., and M. Ritzwoller (2002), Monte Carlo inversion for a global shear velocity model of the crust and upper mantle, *Geophys. J. Int.*, *151*, 88–105.

Sorrells, G., J. Bonner, and E. Herrin (2002), Seismic precursors to space shuttle shock fronts, *Pure Appl. Geophys.*, *159*, 1153–1181.

Toon, O., K. Zahnle, D. Morrison, R. Turco, and C. Covey (1997), Environmental perturbations caused by the impacts of asteroids and comets, *Rev. Geoph.*, *35*, 41–78.

Tromp, J., et al. (2010), Near real-time simulations of global CMT earthquakes, *Geophys. J. Int.*, *183*, 381–389.